Chemical Science

ROYAL SOCIETY OF CHEMISTRY

EDGE ARTICLE

View Article Online
View Journal | View Issue

Cite this: *Chem. Sci.*, 2025, **16**, 4749

All publication charges for this article have been paid for by the Royal Society of Chemistry

"All-four-in-one": a novel mercury tellurite–nitrate $Hg_3(TeO_3)(Te_3O_7)(NO_3)_2$ exhibiting exceptional optical anisotropy†

Ru-Ling Tang, * Yi-Lei Lv, Liang Ma, Bing-Wei Miao, Wenlong Liu and Sheng-Ping Guo *

Received 2nd December 2024
Accepted 1st February 2025

DOI: 10.1039/d4sc08166h

rsc.li/chemical-science

In recent years, birefringent crystals have attracted much attention in the field of optical materials and play a significant role in laser technology and optical imaging. However, commercially available birefringent crystals are still relatively scarce and need improvement. Low-dimensional structures and well-oriented anisotropic units are conducive to obtaining excellent birefringent materials. Therefore, it is crucial to utilize a molecular engineering strategy for designing crystal structures. Through screening, the tellurite–nitrate system caught our attention because most of them exhibit low dimensional structures. The structure of $Hg_3(TeO_3)(Te_3O_7)(NO_3)_2$ (HTTN) consists of unprecedented $[(Hg_3Te_4O_{10})^{2+}]_\infty$ cationic layers built by a $[TeO_3]^{2-}$ triangular pyramid, $[(Te_3O_7)^{2-}]_\infty$ chains, and novel $[(Hg_3O_7)^{8-}]_\infty$ chains balanced by isolated NO_3^- anions. Here, HTTN with multiple functional units was obtained. HTTN has a birefringence value of 0.295 @ 546 nm, which is significantly higher than those of all commercially available birefringent crystals and exhibits the highest value among tellurite–nitrate birefringent crystals. Structural analysis and theoretical calculations reveal that the synergistic interaction between $[TeO_3]^{2-}$ (5.19%) and $[NO_3]^-$ (7.32%) groups and $[(Te_3O_7)^{2-}]_\infty$ (36%) and $[(Hg_3O_7)^{8-}]_\infty$ (51.49%) chains plays a crucial role in the optical anisotropy of HTTN. This study demonstrates that introducing functional units with high optical anisotropy is an effective strategy for developing high-performance birefringent materials.

Introduction

Birefringent crystals have attracted widespread attention in the field of optical materials due to their ability to modulate light polarization. Since the first observation of birefringence, these functional crystals have become indispensable components in various linear optical devices and play a significant role in modern optoelectronic technology.[1] Currently, commercially available birefringent crystals include MgF_2,[2] α-BaB_2O_4,[3] YVO_4,[4] TiO_2,[5] $LiNbO_3$ (ref. 6) and $CaCO_3$.[7] However, these materials have some defects such as a small birefringence effect, susceptibility to phase transitions and cracking, difficulty in processing and a low laser damage threshold.[1g] Therefore, there is an urgent need to develop new high-performance ones.

From the structural perspective, the large birefringence of most commercial birefringent crystals is primarily composed of π conjugated and highly distorted structural units. Besides, low-dimensional structures, particularly one-dimensional (0D) and two-dimensional (2D) structures, have a positive effect on enhancing optical anisotropy.[1h,j] Therefore, it is crucial to utilize molecular engineering to design structures effectively. The presence of lone pair electrons allows cations to form highly distorted polyhedra, which not only exhibit significant anisotropic polarization but also effectively prevent connections with other groups on the same side, thus facilitating the formation of low-dimensional structures,[8] such as Pb_2BO_3Cl, Sn_2PO_4I, and $K_2Sb(P_2O_7)F$.[9] In addition, the presence of planar anionic groups is beneficial for the development of well-performing birefringent materials with low-dimensional structures, including π-conjugated groups such as $(C_3N_6H_8)PbBr_4$, $Ba(H_2C_6N_7O_3)_2\cdot 8H_2O$, $LiRb(HC_3N_3O_3)\cdot 2H_2O$, $Be_2(BO_3)(IO_3)$, $Sr_3Y[PO_4][CO_3]_3$, Sn_2BO_3I, $Sn_2B_5O_9Br$, and $LiZn(OH)CO_3$.[10] Obviously, inorganic π-conjugated BO_3 and CO_3 groups have positive impact on birefringence. NO_3 is very similar to BO_3 and CO_3, but there has been relatively less research on it despite its larger polarizability anisotropy.[11] Furthermore, the combination of lone pairs of nitrate ions helps form compounds with larger birefringence, such as $Pb_2(BO_3)(NO_3)$[12] and $Bi_3TeO_6OH(NO_3)_2$.[13] In order to obtain compounds that can combine distorted lone-pair cation (Pb^{2+}, Se^{4+}, Sn^{2+}, Te^{4+}, *etc.*)-centered polyhedra and nitrate ions and exhibit low-dimensional structures, we screened the existing system (low-dimensional structures especially 1D or 2D and easy to combine with lone-pair

School of Chemistry and Chemical Engineering, Yangzhou University, 180 Siwangting Road, Yangzhou 225002, P. R. China. E-mail: rltang@yzu.edu.cn; spguo@yzu.edu.cn

† Electronic supplementary information (ESI) available: The experimental section and additional tables and figures. CCDC 2400692. For ESI and crystallographic data in CIF or other electronic format see DOI: https://doi.org/10.1039/d4sc08166h

cations). Through research, it has been discovered that the tellurite–nitrate system shows great potential in birefringent performance. Currently, there are only eleven tellurite–nitrates, among which low-dimensional structures account for as high as 80% (Table S5†). These results suggest that tellurite–nitrite salts have great potential in generating crystals with large birefringence characteristics. However, currently only $(SbTeO_3)(NO_3)$ exhibits birefringence with a value of 0.078 at a wavelength of 546 nm,[14a] indicating that there is still significant room for expansion in the study of birefringence for this system.

In recent years, many preeminent Hg-based birefringent crystals have been acquired, including $BaHgSe_2$, $Hg_4(Te_2O_5)(SO_4)$, and $HgBr_2$.[15] It is worth noting that Hg^{2+} ions can adopt various coordination geometries including linear, planar triangular or tetrahedra, providing diversity in structural variations. Furthermore, the significant distortion degree of Hg^{2+} ions contributes to the formation of large birefringence. Therefore, our main research focuses on introducing Hg^{2+} ions into the tellurite–nitrate system.

Based on the above thoughts, this study successfully prepared a novel mercury-based tellurite–nitrate $Hg_3(TeO_3)(Te_3O_7)(NO_3)_2$ (HTTN) containing multiple functional units. It exhibits excellent birefringence. Combined with theoretical calculations, this paper presents the synthesis method, crystal structure and its relevant comparisons, optical properties, and structure–property relationships of $Hg_3(TeO_3)(Te_3O_7)(NO_3)_2$.

Results and discussion

Using TeO_2, $Hg(NO_3)_2\cdot H_2O$, ZnO, and HNO_3 as raw materials, transparent colorless HTTN single crystals were successfully synthesized through a hydrothermal reaction at 200 °C (ESI† for more details). The powder X-ray diffraction (PXRD) characterization result shown in Fig. S1† demonstrates good agreement with the simulated one, confirming the purity. The chemical composition was further supported by EDS elemental analysis presented in Fig. S2.†

$Hg_3(TeO_3)(Te_3O_7)(NO_3)_2$ belongs to the orthorhombic crystal system with the *Pnma* space group (No. 62). The asymmetric unit consists of three Hg, three Te, two N, and twelve O atoms (Fig. S6a†). In the crystal structure, each N atom is coordinated with three O atoms to form a NO_3 planar triangular geometry (Fig. S6a†). The bond distances of N–O are from 1.18(2) to 1.28(2) Å, and the O–N–O bond angles are between 118.4(18) and 122.3(17)°. Hg(1) forms a HgO_5 triangular prism, whereas Hg(2) forms a HgO_4 tetrahedron. Two HgO_4 and one HgO_5 units are combined through the O(3) and O(5) atoms to form a $[Hg_3O_9]$ trimer. Subsequently, the $[Hg_3O_9]$ units connect with each other along the *b*-axis through sharing O atoms to form an S-shaped $[(Hg_3O_7)^{8-}]_\infty$ chain (Fig. 1a). The chains are arranged consistently on the ab plane and stacked along the *c*-axis (Fig. S7a†). Specifically, this is the first discovery of the $[Hg_3O_9]$ trimer and $[(Hg_3O_7)^{8-}]_\infty$ chain. The distances of Hg–O bonds range from 2.11(8) to 2.578(8) Å. The distances of Hg–O bonds range from 2.11(8) to 2.578(8) Å, and the angle of O–Hg–O ranges from 63.2(3) to 170.1(4)°. Both Te(1) and Te(2) atoms are connected to four O atoms, forming TeO_4 tetrahedra. The Te(3) atom is connected to three O atoms, forming a TeO_3 triangular pyramid. It is arranged in an inverted parallel manner in the ab plane and extends infinitely along the *c* axis (Fig. 1b and S7b†). The distances of Te–O bonds range from 1.877(8) to 2.349(2) Å, and the O–Te–O bond angles range from 82.7(8) to 153.9(4)°. All bond lengths and angles observed in this compound are very similar to those found in other compounds. The TeO_3 units, $[(Te_3O_7)^{2-}]_\infty$ chains, and $[(Hg_3O_7)^{8-}]_\infty$ chains are connected together to form wrinkled $[(Hg_3Te_4O_{10})^{2+}]_\infty$ layers in the bc plane, with NO_3^- ions between the layers to balance the charge (Fig. 1d and e). Interestingly, the $[Te_3O_7]^{2-}$ chain, $[Hg_3O_7]^{8-}$ chain, and $[TeO_3]^{2-}$ unit form a collective arrangement that remains nearly coplanar (Fig. 1d). In the $[(Hg_3O_7)^{8-}]_\infty$ chain, Hg atoms are in the same plane (Fig. 1a), while Te^{4+} cations in both the $[TeO_3]^{2-}$ and $[TeO_4]^{4-}$ units are roughly aligned along the *b*-axis (Fig. S7b†). Meanwhile, the NO_3 ions maintain a coplanar arrangement along the ac or bc plane with different orientation

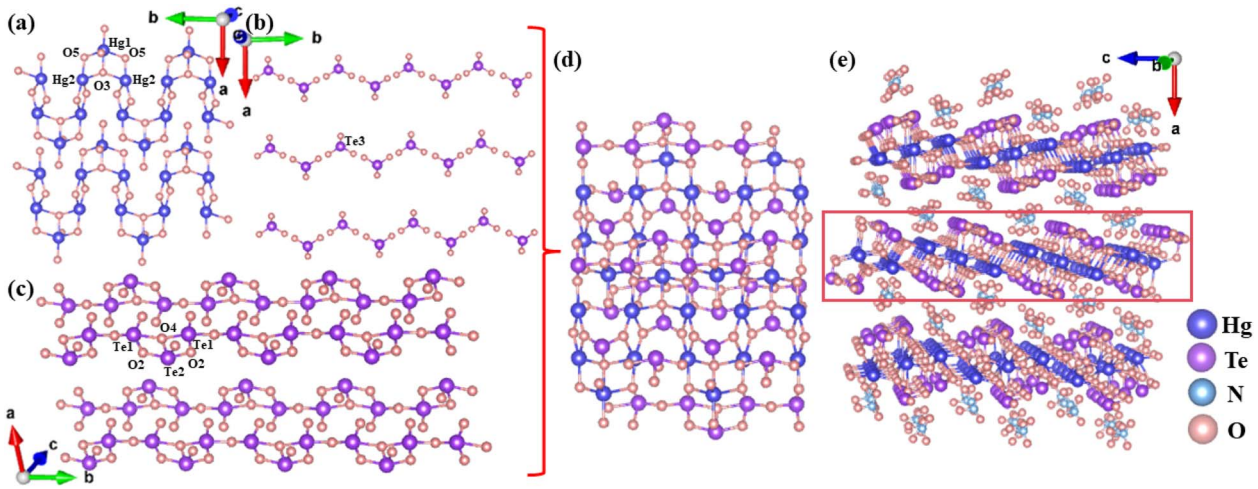

Fig. 1 (a) The $[(Hg_3O_7)^{8-}]_\infty$ chain; (b) the TeO_3 units; (c) the $[(Te_3O_7)^{2-}]_\infty$ chain; (d) the $[(Hg_3Te_4O_{10})^{2+}]_\infty$ layer; and (e) the whole crystal structure of $Hg_3(TeO_3)(Te_3O_7)(NO_3)_2$.

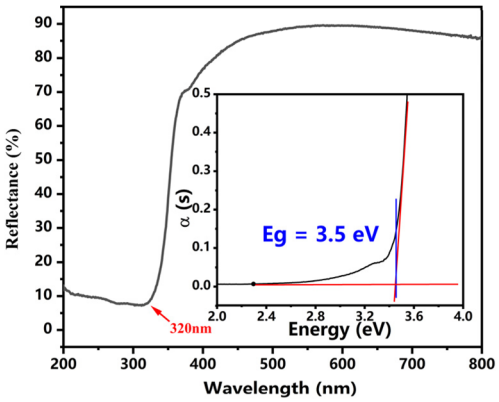

Fig. 2 UV-vis-NIR diffuse reflectance spectra and the optical band gaps obtained from Tauc plots (inset) of $Hg_3(TeO_3)(Te_3O_7)(NO_3)_2$.

modes (Fig. S6b†). The arrangements of these structural units are conducive to strong optical anisotropy.

So far, only eleven tellurite–nitrates have been reported (Table S5†). Furthermore, only $(SbTeO_3)(NO_3)$ has been studied with birefringent performance,[14a] with a value less than 0.1. For tellurite–nitrates with 2D structures, in $(SbTeO_3)(NO_3)$,[14a] $AgTeO_2NO_3$,[14b] $[Bi(TeO_3)](NO_3)$,[16a] $(Te_2O_4)(HNO_3)$,[14e] and $YCu(TeO_3)_2(NO_3)(H_2O)_3$,[14d] the NO_3 ions mainly exist between layers. For 2D $RE(TeO_3)(NO_3)$ (RE = La, Nd, Eu, Gd, Dy, Er and Y),[16b] 0D $Ca_5Te_4O_{12}(NO_3)_2(H_2O)_2$ and 3D $Ca_6Te_5O_{15}(NO_3)_2$,[16c] the NO_3^- groups are connected to the cations RE^{3+} and Ca^{2+}, respectively. In 0D $Bi_3(\mu_3\text{-}OH)(TeO_3)_3(NO_3)_2$ (ref. 16d) and H $[Bi_3O(Te_3O_9)](NO_3)_2$,[14c] the NO_3 units are free between chains. It can be seen that different positions of NO_3^- lead to significant changes in structural dimensions which may affect birefringence. In the above compounds, Te atoms exhibit different coordination forms: TeO_2, TeO_3, and TeO_4 units. Additionally, there are Te_2O_2 rings and $[(Te_3O_{10})^{8-}]_\infty$, $(TeO_2)_\infty$ and $[(TeO_4)^{4-}]_\infty$ chains. Obviously, $Hg_3(TeO_3)(Te_3O_7)(NO_3)_2$ includes both TeO_3 and TeO_4 units along with $[(Te_3O_7)^{2-}]_\infty$ chain in the tellurate–nitrate system for the first time. Simultaneously, the existence of Hg_3O_9 units and $[(Hg_3O_7)^{8-}]_\infty$ chains is also observed for the first time.

Fig. S3† shows the TG curves of HTTN, which suggest that HTTN can be stable below 373 °C, more stable than $Bi_3(\mu_3\text{-}OH)(TeO_3)_3(NO_3)_2$ (180 °C),[16d] $(SbTeO_3)(NO_3)$ (273 °C),[14a] and $[Bi(TeO_3)](NO_3)$ (370 °C).[16a]

The optical band gap of HTTN was determined to be 3.5 eV based on UV-vis-NIR diffuse reflectance spectroscopy and the Kubelka–Munk function (Fig. 2). The band gap value is higher than that of $Bi_3(\mu_3\text{-}OH)(TeO_3)_3(NO_3)_2$ (3.31 eV) and $H[Bi_3O(Te_3O_9)](NO_3)_2$ (3.26 eV).[16d,14c] The infrared spectrum and vibration peak distribution of HTTN are shown in Fig. S5.† There are no obvious vibration peaks in the range of 1500–4000 cm^{-1}. The strong bands at 1401 and 1295 cm^{-1} correspond to the N–O stretching vibrations of the triangular NO_3 group, while those at 1039 and 817 cm^{-1} correspond to non-planar bending vibrations of the NO_3 plane group. The peaks at 759 and 696 cm^{-1} can be attributed to Te–O stretching, while those at 609 and 518 cm^{-1} can be attributed to symmetric and asymmetric stretching of Hg–O bonds. These vibration peaks are close to those in the literature.[17]

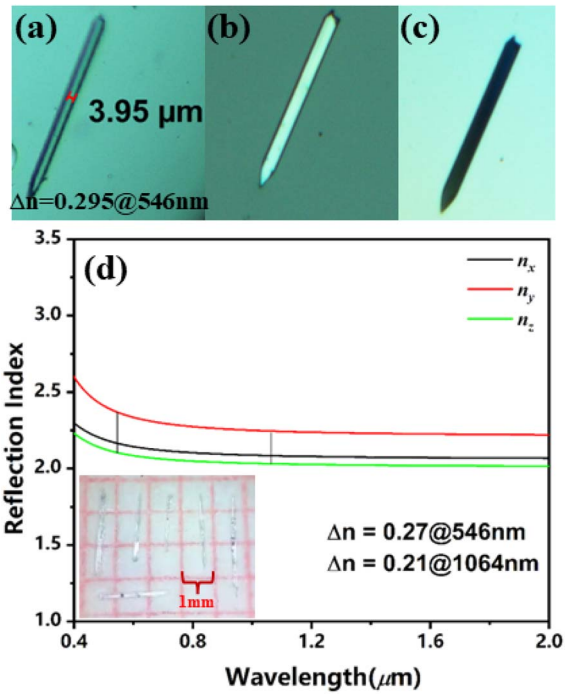

Fig. 3 (a) Experimental birefringence at 546 nm. (b) Polarization optical microscope image of a $Hg_3(TeO_3)(Te_3O_7)(NO_3)_2$ single crystal. (c) A single crystal corresponding to complete extinction. (d) Calculated refractive index dispersion curves of $Hg_3(TeO_3)(Te_3O_7)(NO_3)_2$.

In order to further investigate the potential of $Hg_3(TeO_3)(Te_3O_7)(NO_3)_2$ as a birefringent material, its birefringence was measured using a polarizing microscope equipped with a 546 nm light source. The thickness of the crystal was 3.95 μm, and the optical path difference at a wavelength of 546 nm was determined to be 1.16684 μm (Fig. 3b and c).[14a] According to the formula "$R = \Delta n \times T$", the birefringence can be calculated. The result showed that the birefringence of $Hg_3(TeO_3)(Te_3O_7)(NO_3)_2$ at 546 nm is 0.295 (Fig. 3a). A statistical analysis on all inorganic

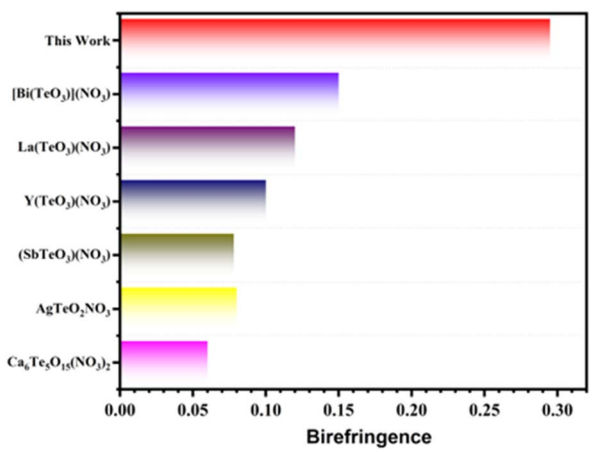

Fig. 4 Birefringence of tellurite–nitrate crystals.

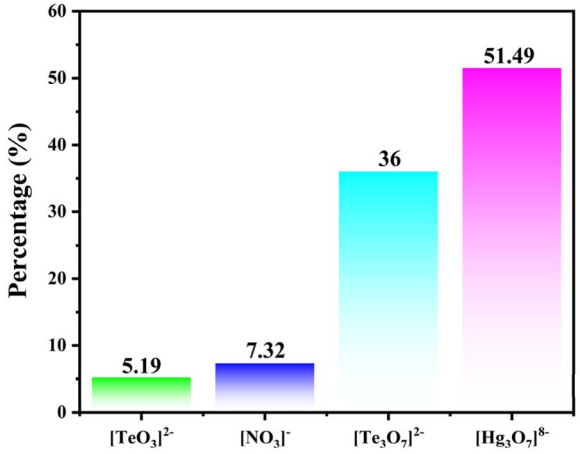

Fig. 5 Calculated birefringence contribution from $[TeO_3]^{2-}$, $[NO_3]^-$ groups, $[Te_3O_7]^{2-}$, and $[Hg_3O_7]^{8-}$ chains.

nitrates with experimentally determined birefringence was performed, and the results show that $Hg_3(TeO_3)(Te_3O_7)(NO_3)_2$ shows higher birefringence compared with $Pb_6O_4(BO_3)(NO_3)$ (0.276 @ 546 nm), $In(IO_3)_2(NO_3)$ (0.268 @ 546 nm), $[Al(H_2O)_6](IO_3)_2(NO_3)$ (0.252 @ 546 nm), $Pb_6O_2(BO_3)_2(NO_3)F$ (0.241 @ 546 nm), *etc.*[18] Additionally, the birefringence of $Hg_3(TeO_3)(Te_3O_7)(NO_3)_2$ exceeds that of commercially available α-BaB_2O_4 (0.122 @ 546 nm),[3] $CaCO_3$ (0.172 @ 546 nm),[7] YVO_4 (0.204 @ 532 nm),[4] TiO_2 (0.256 @ 546 nm),[5] and some other common birefringent crystals (Table S4†). Furthermore, its birefringence value surpasses that of all known birefringence tellurite–nitrates, being 3.78 times greater than $(SbTeO_3)(NO_3)$ (0.078 @ 546 nm) (Fig. 4 and S8†).[14a] In conclusion, $Hg_3(TeO_3)(Te_3O_7)(NO_3)_2$ shows great potential as a birefringent material.

In order to accurately elucidate the relationship between the structure and performance, first-principles calculations were conducted. The results show that $Hg_3(TeO_3)(Te_3O_7)(NO_3)_2$ exhibits a direct band gap of 2.4 eV (Fig. S4a†). Due to the limitation of the GGA-PBE method, the calculated band gap value is underestimated compared to experimental values.[1i,j] Therefore, we used a scissor operator of 1.1 eV to evaluate the optical properties of $Hg_3(TeO_3)(Te_3O_7)(NO_3)_2$. The density of states distribution for $Hg_3(TeO_3)(Te_3O_7)(NO_3)_2$ is shown in Fig. S4b,† where the top region of the valence band is mainly occupied by O-2p and Hg-5d orbitals and some Te-5s and Te-5p orbitals. The bottom region of the conduction band is primarily filled with O-2p, Te-5p, Hg-6s and some N-2p orbitals. From this it can be inferred that charge transfer between valence and conduction bands is mainly determined by Hg, Te, and O atoms. It can be found from the valence band to the conduction band that there is a strong overlap between the electronic states of Te and Hg atoms with those of O atoms, indicating a strong interaction between Te–O and Hg–O bonds. To further

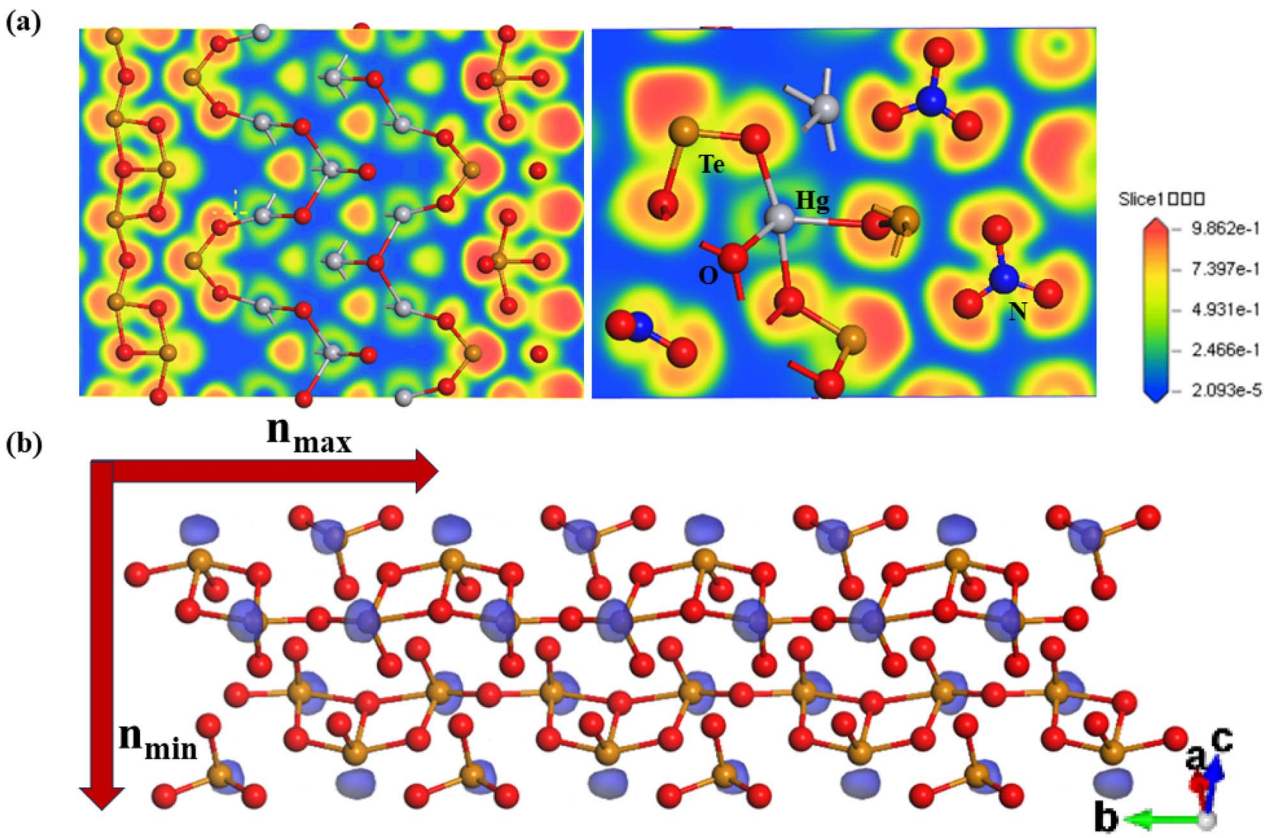

Fig. 6 (a) The electron localization function diagram. (b) Arrangement of the $[TeO_3]^{2-}$ unit and $[Te_3O_7]^{2-}$ chains in $Hg_3(TeO_3)(Te_3O_7)(NO_3)_2$. Blue crescents indicate the approximate position of lone-pair electrons. The downward and rightward arrows respectively represent the minimum and maximum refractive indices along the *c*-axis and *b*-axis directions.

confirm the origin of the birefringence, an atom-resolved birefringence analysis was conducted. The birefringence in $Hg_3(TeO_3)(Te_3O_7)(NO_3)_2$ is attributed to $[TeO_3]^{2-}$ (5.19%), $[NO_3]^-$ (7.32%) groups, $[Te_3O_7]^{2-}$ (36%) , and $[Hg_3O_7]^{8-}$ (51.49%) chains. This further confirms that the synergistic strategy involving four functional groups results in the compound possessing significant birefringence (Fig. 5).[19]

$Hg_3(TeO_3)(Te_3O_7)(NO_3)_2$ crystallizes in the orthorhombic crystal system and belongs to the biaxial crystal system, with three refractive indices (n_x, n_y, and n_z) along the x, y, and z axes respectively. The refractive indices of $Hg_3(TeO_3)(Te_3O_7)(NO_3)_2$ satisfy the relationship $n_y > n_x > n_z$. According to theoretical calculations, the birefringence value Δn at a wavelength of 546 nm is determined to be 0.27, which is close to the experimental result (Fig. 3d).

In order to gain a deeper understanding of the contributions of different functional groups to the optical anisotropy of $Hg_3(TeO_3)(Te_3O_7)(NO_3)_2$, we calculated the electron localization function maps for $Hg_3(TeO_3)(Te_3O_7)(NO_3)_2$. According to Fig. 6, obvious distortion can be observed in the electron clouds surrounding the $[TeO_3]^{2-}$ and $[NO_3]^-$ groups, as well as the $[(Te_3O_7)^{2-}]_\infty$ and $[(Hg_3O_7)^{8-}]_\infty$ chains. According to the research by Pan's team, the contribution of lone pairs to birefringence becomes more significant as $\cos\theta$ (the angle between the direction of lone pairs and the optical axis n_{min}) increases.[20] Fig. 6b shows that when lone pair electrons are parallel to the optical axis n (determined by selecting the refractive index with the smallest value among the three axes calculated using DFT), the $\cos\theta$ factor is 1. Therefore, observing TeO_3 and Te_3O_7 units with directions of lone pair electrons in this compound helps observe larger birefringence. Therefore, it can be concluded from further analysis of $Hg_3(TeO_3)(Te_3O_7)(NO_3)_2$ difference charge density maps that prominent optical anisotropy mainly arises from a synergistic interaction among the $[TeO_3]^{2-}$ and $[NO_3]^-$ groups, as well as the $[(Te_3O_7)^{2-}]_\infty$ and $[(Hg_3O_7)^{8-}]_\infty$ chains.

Conclusions

In conclusion, we successfully synthesized a novel mercury-based tellurite–nitrate $Hg_3(TeO_3)(Te_3O_7)(NO_3)_2$. $Hg_3(TeO_3)(Te_3O_7)(NO_3)_2$ is the first tellurite–nitrate compound generated by multiple functional units that exhibits excellent optical anisotropy. It possesses a unique crystal structure composed of $[TeO_3]$ triangular pyramids, $[NO_3]^-$ units, $[(Te_3O_7)^{2-}]_\infty$ chains, and $[(Hg_3O_7)^{8-}]_\infty$ chains. The research results indicate that $Hg_3(TeO_3)(Te_3O_7)(NO_3)_2$ possesses a wide bandgap (3.5 eV) and an excellent birefringence (0.295 @ 546 nm). This represents the largest birefringence in tellurite–nitrate, surpassing that of commercially available birefringent crystals. Additionally, theoretical calculations and structural analysis indicate that the synergistic interactions between $[TeO_3]^{2-}$ and $[NO_3]^-$ groups, as well as between $[(Te_3O_7)^{2-}]_\infty$ and $[(Hg_3O_7)^{8-}]_\infty$ chains, are the main factors causing the optical anisotropy. This work significantly enriches the family of nitrate compounds and has important implications for further understanding and exploring nitrate crystal structures and developing high-quality birefringent materials. It provides new insights for future design and research on excellent birefringent materials.

Data availability

The data supporting this article have been included as part of the ESI.†

Author contributions

This work was conceptualised by Ru-Ling Tang. Experimentation was performed by Yi-Lei Lv and Ru-Ling Tang. Software analysis was performed by Liang Ma. Bing-Wei Miao has experimental assisted contribution. Wenlong Liu contributed supervision. Besides, Ru-Ling Tang and Sheng-Ping Guo contributed funding acquisition and supervision. The first draft of the manuscript was prepared by Ru-Ling Tang and Yi-Lei Lv, and the final draft was edited by all the authors.

Conflicts of interest

The authors declare no competing financial interests.

Acknowledgements

The authors acknowledge the financial support from the National Natural Science Foundation of China (22101248), the Lvyangjinfeng Talent Program of Yangzhou (YZLYJFJ-H2021YXBS083), and the Qinglan Project of Yangzhou University.

Notes and references

1 (*a*) S. Niu, G. Joe, H. Zhao, Y. Zhou, T. Orvis, H. Huyan, J. Salman, K. Mahalingam, B. Urwin, J. Wu, Y. Liu, T. E. Tiwald, S. B. Cronin, B. M. Howe, M. Mecklenburg, R. Haiges, D. J. Singh, H. Wang, M. A. Kats and J. Ravichandran, *Nat. Photonics*, 2018, **12**, 392–396; (*b*) G. A. Ermolaev, D. V. Grudinin, Y. V. Stebunov, K. V. Voronin, V. G. Kravets, J. Duan, A. B. Mazitov, G. I. Tselikov, A. Bylinkin, D. I. Yakubovsky, S. M. Novikov, D. G. Baranov, A. Y. Nikitin, I. A. Kruglov, T. Shegai, P. Alonso-González, A. N. Grigorenko, A. V. Arsenin, K. S. Novoselov and V. S. Volkov, *Nat. Comm.*, 2021, **12**, 854; (*c*) N. A. Rubin, G. D'Aversa, P. Chevalier, Z. Shi, W. T. Chen and F. Capasso, *Science*, 2019, **365**, 43; (*d*) X. H. Meng, W. L. Yin and M. J. Xia, *Coord. Chem. Rev.*, 2021, **439**, 213916; (*e*) R. L. Tang, D. X. Yang, L. Ma, Y. L. Lv, W. L. Long and S. P. Guo, *Adv. Opt. Mater.*, 2024, DOI: 10.1002/adom.202403044; (*f*) A. Tudi, S. Han, Z. Yang and S. L. Pan, *Coord. Chem. Rev.*, 2022, **459**, 214380; (*g*) Y. Q. Li, X. Zhang, J. Y. Zheng, Y. Zhou, W. Q. Huang, Y. P. Song, H. Wang, X. Y. Song, J. H. Luo and S. G. Zhao, *Angew. Chem., Int. Ed.*, 2023, **62**, e202304498; (*h*) T. Wu, X. Jiang, K. Duanmu, C. Wu, Z. Lin, Z. Huang, M. G. Humphrey and C. Zhang, *Adv. Sci.*, 2024, **11**, 2470070; (*i*) Y. W. Kang and Q. Wu, *Coord. Chem. Rev.*,

2024, **498**, 215458; (*j*) Y. Zhou, Z. F. Guo, H. G. Gu, Y. Q. Li, Y. P. Song, S. Y. Liu, M. C. Hong, S. G. Zhao and J. H. Luo, *Nat. Photonics*, 2024, **18**, 922–927; (*k*) J. Chen, M. B. Xu, H. Y. Wu, J. Y. Wu and K. Z. Du, *Angew. Chem., Int. Ed.*, 2024, **136**, e202411503.

2 M. J. Dodge, *Appl. Opt.*, 1984, **23**, 1980–1985.

3 X. J. Zhou Guoqing, X. Chen, H. Zhong, S. Wang, K. Xu, D. Peizhen and G. Fuxi, *J. Cryst. Growth*, 1998, **191**, 517–519.

4 T. T. H. T. Luo and E. L. Dereniak, *Opt. Lett.*, 2006, **31**, 616.

5 W. M. SINTON, *J. Opt. Soc. Am.*, 1961, **51**, 1309.

6 D. E. Zelmon, D. L. Small and D. Jundt, *J. Opt. Soc. Am. B*, 1997, **14**, 3319–3322.

7 G. Ghosh, *Opt. Commun.*, 1999, **163**, 95–102.

8 L. Y. Ren, L. H. Cheng, X. Y. Zhou, J. X. Ren, L. L. Cao, L. Huang, X. H. Dong, Y. Q. Zhou, D. J. Gao and G. H. Zou, *Inorg. Chem. Front.*, 2023, **10**, 5602–5610.

9 (*a*) G. H. Zou, C. S. Lin, H. Jo, G. Nam, T. S. You and K. M. Ok, *Angew. Chem., Int. Ed.*, 2016, **55**, 12078–12082; (*b*) J. Y. Guo, A. Tudi, S. J. Han, Z. H. Yang and S. L. Pan, *Angew. Chem., Int. Ed.*, 2021, **60**, 24901–24904; (*c*) S. V. Krivovichev and L. Bindi, *Angew. Chem., Int. Ed.*, 2020, **60**, 3854–3855.

10 (*a*) Q. T. Xu, Z. Y. Wang, Y. Zhou, W. Q. Huang, Y. P. Song, J. Y. Zeng, L. Y. Qiang, L. X. Hou, J. H. Luo and S. G. Zhao, *Adv. Funct. Mater.*, 2024, 2417431; (*b*) Y. Q. Li, W. Q. Huang, Y. Zhou, X. Y. Song, J. Y. Zheng, H. Wang, Y. P. Song, M. J. Li, J. H. Luo and S. G. Zhao, *Angew. Chem., Int. Ed.*, 2022, **62**, 202215145; (*c*) J. Lu, Y. K. Lian, L. Xiong, Q. R. Wu, M. Zhao, K. X. Shi, L. Chen and L. M. Wu, *J. Am. Chem. Soc.*, 2019, **141**, 16151; (*d*) G. Peng, C. S. Lin, H. X. Fan, K. C. Chen, B. X. Li, G. Zhang and N. Ye, *Angew. Chem., Int. Ed.*, 2021, **60**, 17415–17418; (*e*) L. Xiong, L. M. Wu and L. Chen, *Angew. Chem., Int. Ed.*, 2021, **60**, 25063–25067; (*f*) J. Y. Guo, S. C. Cheng, S. J. Han, Z. H. Yang and S. L. Pan, *Adv. Opt. Mater.*, 2021, **9**, 2001734; (*g*) X. M. Liu, L. Kang, P. F. Gong and Z. S. Lin, *Angew. Chem., Int. Ed.*, 2021, **60**, 13574–13578.

11 H. X. Fan, M. Luo and N. Ye, *J. Synth. Cryst.*, 2022, **51**, 1588–1597.

12 J. L. Song, C. L. Hu, X. Xu, F. Kong and J. G. Mao, *Angew. Chem., Int. Ed.*, 2015, **54**, 3679–3682.

13 S. G. Zhao, Y. Yang, Y. G. Shen, B. Q. Zhao, L. Li, C. M. Ji, Z. Y. Wu, D. Q. Yuan, Z. S. Lin, M. C. Hong and J. H. Luo, *Angew. Chem., Int. Ed.*, 2017, **56**, 540–544.

14 (*a*) B. Zhang, C. L. Hu, J. G. Mao and F. Kong, *Chem. Sci.*, 2024, **15**, 18549–18556; (*b*) C. Olsson, L. G. Johansson and S. Kazikowski, *Acta Crystallogr., Sect. C:Cryst. Struct. Commun.*, 1988, **44**, 427–429; (*c*) C. L. Sun, D. J. Mei, J. L. Xu and Y. D. Wu, *J. Alloys Compd.*, 2017, **702**, 410–417; (*d*) S. J. Mills, M. A. Dunstan and A. G. Christy, *Acta Crystallogr.*, 2016, **E72**, 1138–1142; (*e*) L. N. Swink and G. B. Carpenter, *Acta Crystallogr.*, 1966, **21**, 578.

15 (*a*) C. Li, W. L. Yin, P. F. Gong, X. S. Li, M. L. Zhou, A. Mar, Z. S. Lin, J. Y. Yao, Y. C. Wu and C. T. Chen, *J. Am. Chem. Soc.*, 2016, **138**, 6135–6138; (*b*) P. F. Li, C. L. Hu, Y. F. Li, J. G. Mao and F. Kong, *J. Am. Chem. Soc.*, 2024, **146**, 7868–7874; (*c*) M. S. Zhang, W. D. Yao, S. M. Pei, B. W. Liu, X. M. Jiang and G. C. Guo, *Chem. Sci.*, 2024, **15**, 6891–6896.

16 (*a*) C. Y. Meng, M. F. Wei, L. Geng, P. Q. Hu, M. X. Yu and W. D. Cheng, *J. Solid State Chem.*, 2016, **239**, 46–52; (*b*) H. E. Lee, H. Jo, M. H. Lee and K. M. Ok, *J. Alloys Compd.*, 2021, **851**, 156855; (*c*) B. Stoge and M. Weil, *Mineral. Petrol.*, 2013, **107**, 253–263; (*d*) J. L. Song and C. Qian, *ChemistrySelect*, 2017, **2**, 1681–1685.

17 (*a*) L. Qi, X. X. Jiang, K. N. Duanmu, C. Wu, Z. S. Lin, Z. P. Huang, M. G. Humphrey and C. Zhang, *Angew. Chem., Int. Ed.*, 2023, **62**, e202309365; (*b*) Y. L. Lv, L. Huai, Y. L. Wei, L. Ma, Y. Q. Wei, W. L. Liu and R. L. Tang, *Inorg. Chem. Front.*, 2023, **10**, 4845–4853.

18 (*a*) S. Bai, D. Q. Yang, B. B. Zhang, L. Li and Y. Wang, *Dalton Trans.*, 2022, **51**, 3421–3425; (*b*) Y. Huang, T. K. Jiang, B. P. Yang, C. L. Hu, Z. Fang and J. G. Mao, *Inorg. Chem.*, 2022, **61**, 3374–3378; (*c*) D. K. Smith, M. N. Bello, D. K. Unruh and M. L. Pantoya, *Combust. Flame*, 2017, **179**, 154–156; (*d*) G. Peng, Y. Yang, Y. H. Tang, M. Luo, T. Yan, Y. Q. Zhou, C. S. Lin, Z. S. Lin and N. Ye, *Chem. Commun.*, 2017, **53**, 9398–9401; (*e*) Y. L. Lv, W. Xu, W. D. Yao, M. B. Xu, W. L. Liu, S. P. Guo and R. L. Tang, *Inorg. Chem.*, 2024, **63**, 6127–6173; (*f*) Q. Wang, J. X. Ren, D. Wang, L. L. Cao, X. H. Dong, L. Huang, D. J. Gao and G. H. Zou, *Inorg. Chem. Front.*, 2023, **10**, 2107–2114; (*g*) Y. Long, X. H. Dong, H. M. Zeng, Z. Lin and G. H. Zou, *Inorg. Chem.*, 2022, **61**, 4184–4192; (*h*) Y. X. Song, M. Luo, C. S. Lin and N. Ye, *Chem. Mater.*, 2017, **29**, 896–903; (*i*) Y. Long, X. H. Dong, L. Huang, H. M. Zeng, Z. Lin and G. H. Zou, *Inorg. Chem.*, 2020, **59**, 12578–12585.

19 X. Y. Zhou, X. Mao, P. Zhang, X. H. Dong, L. Huang, L. L. Cao, D. J. Gao and G. H. Zou, *Inorg. Chem. Front.*, 2024, **11**, 3221–3228.

20 (*a*) J. Y. Guo, A. Tudi, S. J. Han, Z. H. Yang and S. L. Pan, *Angew. Chem., Int. Ed.*, 2021, **60**, 3540–3544; (*b*) Y. Huang, Z. Fang, B. P. Yang, X. Y. Zhang and J. G. Mao, *Scr. Mater.*, 2023, **223**, 115082.